Generalizing Similarity Laws for Radio-Frequency Discharge Plasmas across Nonlinear Transition Regimes

Yangyang Fu, Huihui Wang, Bocong Zheng, Peng Zhang, Qi Hua Fan, Xinxin Wang, and John P. Verboncoeur

Phys. Rev. Applied **16**, 054016 — Published 8 November 2021

DOI: 10.1103/PhysRevApplied.16.054016

Generalizing Similarity Laws for Radio Frequency Discharge Plasmas across Nonlinear Transition Regimes

Yangyang Fu,[1] Huihui Wang,[2] Bocong Zheng,[3] Peng Zhang,[4] Qi Hua Fan,[3,4,5] Xinxin Wang,[1] and John P. Verboncoeur[4,6]

[1]*Department of Electrical Engineering, Tsinghua University, Beijing, 100084, China*

[2]*Department of Chemical Engineering, Tsinghua University, Beijing, 100084, China*

[3]*Fraunhofer USA Center Midwest, Michigan State University, East Lansing, Michigan 48824, USA*

[4]*Department of Electrical and Computer Engineering, Michigan State University, East Lansing, Michigan 48824, USA*

[5]*Department of Chemical Engineering and Materials Science, Michigan State University, East Lansing, Michigan 48824, USA*

[6]*Department of Computational Mathematics, Science and Engineering, Michigan State University, East Lansing, Michigan 48824, USA*

(Dated: October 1, 2021; Authors to whom correspondence should be addressed: fuyangyang@tsinghua.edu.cn, bzheng@fraunhofer.org)

We generalize the similarity theory based on the scaling and solution invariance of the Boltzmann equation, coupled with the Poisson equation, and demonstrate similarity laws for radio frequency (rf) discharge plasmas across three nonlinear transitional regimes, namely, the alpha-gamma mode transition, stochastic-Ohmic heating mode transition, and bounced resonance heating mode transition. Fundamental plasma parameters, e.g., electron power absorption, under similar discharge conditions are examined via fully kinetic particle-in-cell simulations, and further the electron kinetic invariance is exemplified in similar rf discharge plasmas. The results from this work unambiguously confirm the applicability of similarity laws for rf plasma toward extended operating regimes, and strengthen the foundation and framework of similarity physics with universality.

I. INTRODUCTION

Similarity laws map out how discharge conditions change to retain the same characteristics [1–4], which have been explored and demonstrated from laboratory to nature discharge phenomena, such as glow discharges [5, 6], streamers [7], pulsed electrical breakdown [8, 9], fusion plasmas [10], and mesosphere red-sprite discharges [11, 12]. The studies on gas discharge similarities can date back to those by Paschen [13] and Townsend [14], which initiated the usage of combined parameters, such as the reduced gap length *pd* (gas pressure times gap distance) and reduced electric field E/p (electric field divided by gas pressure) for characterizing discharge behaviors, e.g., Townsend coefficient with local-field approximation describing the ionization process under direct current (dc) voltage. Historically, most of the initial similarity investigations are for dc discharges while in 1948 Margenau [15] theoretically showed the similarity principle for high frequency discharges. He proposed an additional combined parameter, reduced frequency f/p (driving frequency divided by gas pressure), which was later experimentally verified by Jones and Morgan [16]. In 2008 Lisovskiy *et al.* [17] experimentally validated the breakdown similarity laws, e.g., Paschen's law [13], for radio frequency (rf) discharges in both atomic and molecular gases, including argon, nitrogen, and hydrogen. Nowadays due to the widespread applications of the rf discharge plasmas [18, 19], it is of fundamental importance to elucidate the applicability of similarity laws toward more comprehensive discharge regimes, which is essential for correlating discharge parameters among rf plasma systems at different dimension scales.

In more recent years, Puač *et al.* [20] and Lee *et al.* [21] demonstrated breakdown similarity laws in rf discharge at macro and micro scales, respectively. Loveless *et al.* [22] conducted nondimensionalized equation analysis on gas breakdown under rf and microwave driven electric fields and inferred the universality of scaling laws for alternating current (ac) gas breakdown. Very recently, rather than using a fluidic method with the local-field approximation, Fu *et al.* [23] further confirmed the similarity of the alpha mode capactive rf plasmas in nonlocal kinetic regimes through particle simulations. However, understandings of the discharge similarity laws are still far from complete, for example, up to date, the effects of nonlinear physical mechanisms on discharge similarities are rarely investigated and the applicability of similarity laws in rf discharge mode transition regimes of rf plasmas, e.g., the alpha-gamma (AG) mode transition [24], the stochastic-Ohmic (SO) heating mode transition [25, 26], and the bounced resonant heating (BRH) mode transition [27–29], has not yet been confirmed, which severely limit the application of the similarity theory.

In this work, we generalize the similarity laws for rf discharge plasmas across the aforementioned three nonlinear transition regimes, i.e., the AG, SO, and BRH mode transitions. Based on fully kinetic particle-in-cell/Monte Carlo collision (PIC/MCC) simulations, the AG, SO, and BRH mode transitions are observed in rf plasmas by tuning the applied rf voltage, gas pressure, and gap distance, respectively, showing distinctive nonlinear parameter scaling relations. By simultaneously manipulating the external discharge condition parameters $[p,d,f]$, we found that the nonlinear characteristics can be exactly replicated under similar discharge conditions, which unambiguously confirmed the validity of similarity laws across the considered nonlinear transition regimes. The results from this work provide additional knobs and more flexibility in characterizing rf discharges across a wider range of parameter regimes, which are essential for the optimization and fabrication of plasma devices.

II. THEORY AND MODEL

Similarity laws are usually utilized for the correlation of discharges in geometrically similar gaps, the linear dimensions of which are proportional in every direction, i.e., $d_{1j} = kd_{kj}$, where $j = [x, y, z]$ represents the coordinate direction, d_1 is the dimension in base (or prototype) case, and d_k is the dimension in a scaled case that, compared to the base case, has a geometrical scaling factor of k. According to the similarity theory [30], a physical parameter $G(x,t)$ at the corresponding spatiotemporal point (x,t) in similar discharge systems can be transformed through

$$G(x_1,t_1) = k^{\alpha[G]} G(x_k,t_k)\,, \tag{1}$$

where the subscripts 1 and k indicate the prototype gap and the scaled gap having a scaling factor of k, respectively; (x_1,t_1) and (x_k,t_k) are the corresponding spatiotemporal points in compared gaps, which are defined by the scaling factor $k = x_1/x_k = t_1/t_k$; and $\alpha[G]$ is the similarity factor for parameter G. Note that the scaling factor k need not be an integer and could be less than one. The most common similarity factors include $\alpha[n_\mathrm{e}] = \alpha[\mathbf{J}_\mathrm{e}] = -2$ for electron density n_e and electron current density $\mathbf{J}_\mathrm{e}$, $\alpha[\mathbf{E}] = \alpha[p] = -1$ for electric field $\mathbf{E}$ and gas pressure p, $\alpha[\varepsilon_\mathrm{e}] = \alpha[\mathbf{v}_\mathrm{e}] = 0$ for electron energy ε_e and electron velocity $\mathbf{v}_\mathrm{e}$, and $\alpha[d] = \alpha[x] = \alpha[t] = 1$ for gap dimension d, position x and time t [31]. Especially, from the transformation in Eq. (1), the parameters having $\alpha[G] = 0$ are similarity invariants, such as the combined parameters E/p and n_e/p^2 [32].

Previously, similarity theory was mostly elaborated within the framework of the local-field or local-energy approximations [15, 33]. However, in low-pressure rf discharge electron kinetics could be highly nonlocal and the local reduced electric field might not be proportional to the electron mean energy, which is a prerequisite of conventional explanations. Here in the following we interpret the similarity laws with a more generalized approach, which is based on the scaling and solution invariance of the Boltzmann equation and coupled with the Poisson equation. Considering the rf plasmas in weakly ionized regimes, the collision is dominated by the electron neutral collision and the Boltzmann equation for electrons can be expressed as

$$\frac{\partial f_\mathrm{e}}{\partial t} + \mathbf{v}\cdot\nabla_\mathbf{x} f_\mathrm{e} - \frac{e\mathbf{E}}{m_\mathrm{e}}\cdot\nabla_\mathbf{v} f_\mathrm{e} = \sum_j C^j_\mathrm{en}[f_\mathrm{e} f_\mathrm{n}, v_\mathrm{en}, \sigma_\mathrm{en}(v_\mathrm{en})]\,, \tag{2}$$

where f_e is the electron distribution function, $\mathbf{v}$ is the velocity, e is the elementary charge, and $C^j_\mathrm{en}[f_\mathrm{e} f_\mathrm{n}, v_\mathrm{en}, \sigma_\mathrm{en}(v_\mathrm{en})]$ is an integral term for the j^th collision between electrons and neutrals, which depends on the relative velocity v_en, the collision cross section $\sigma_\mathrm{en}(v_\mathrm{en})$, and the distributions of electrons and neutrals f_e and f_n [34]. By dividing Eq. (2) with k^3, we have

$$\begin{aligned}\frac{\partial(f_\mathrm{e}/k^2)}{\partial(kt)} &+ \mathbf{v}\cdot\nabla_{(k\mathbf{x})}(f_\mathrm{e}/k^2) - \frac{e(\mathbf{E}/k)}{m_\mathrm{e}}\cdot\nabla_\mathbf{v}(f_\mathrm{e}/k^2) \\ &= \sum_j C^j_\mathrm{en}[(f_\mathrm{e}/k^2)(f_\mathrm{n}/k), v_\mathrm{en}, \sigma_\mathrm{en}(v_\mathrm{en})]\,.\end{aligned} \tag{3}$$

Note that once the compared systems are given, k is a constant and can be put inside the integration of the collision term. By substituting the scaled parameters, i.e., kt, $k\mathbf{x}$, $\mathbf{E}/k$, f_n/k, and f_e/k^2, Eqs. (2) and (3) would demonstrate the solution invariance. Considering Eq. (2) for the base case and Eq. (3) for the scaled system, one can rewrite the parameter relation using Eq. (1) and then obtain $\alpha[t] = \alpha[\mathbf{x}] = 1$, $\alpha[\mathbf{E}] = -1$, $\alpha[f_\mathrm{n}] = -1$, and $\alpha[f_\mathrm{e}] = -2$, which consistently explains the scaling factors for different parameters.

Note that more detailed descriptions of the collision term should be referred to the Boltzmann collision integral or the Fokker-Planck collision term [35]. Since the main collisional processes in a weakly ionized plasma are between charged and neutral particles, here the simultaneous Coulomb interactions between charged particles are not taken into account and beyond the scope of this work. Therefore, we employ a Krook-like relaxation model [35] that can be derived from the simplified Boltzmann collision integral, assuming the neutral distribution f_n stationary and not perturbed by collisions. The relaxation model for the collision term is expressed as $(\delta f_\mathrm{e}/\delta t)_\mathrm{coll} = -\nu_\mathrm{rc}(f_\mathrm{e} - f_\mathrm{e0})$, where $\nu_\mathrm{rc} = \sigma_\mathrm{m} v_\mathrm{en} N_\mathrm{n} \propto p$ is the velocity-dependent relaxation collision frequency, with σ_m the momentum transfer cross section and N_n the neutral gas number density, and f_e0 is the equilibrium distribution function of electrons. In Eq. (3), when the collision term is divided by k^3, since $\alpha[\nu_\mathrm{rc}] = \alpha[p] = -1$, $\alpha[f_\mathrm{e}] = \alpha[f_\mathrm{e0}] = -2$ can be directly concluded with the equation solution invariance. Although the collision term for the inter-particle interactions is simplified, the general idea of the similarity scalings can be straightforwardly demonstrated in a kinetic manner.

From $\alpha[f_\mathrm{e}] = -2$ and $n_\mathrm{e} = \int f_\mathrm{e}(\mathbf{v})\,\mathrm{d}\mathbf{v}$, we can directly obtain the similarity factor for electron density $\alpha[n_\mathrm{e}] = -2$. Further we can also identify the similarity scaling for the Poisson equation, which is expressed as $-\partial(\varepsilon\mathbf{E})/\partial x = e\int[f_\mathrm{e}(\mathbf{v}) - f_\mathrm{i}(\mathbf{v})]\,\mathrm{d}\mathbf{v}$ with ε being the permittivity constant. Here, $\alpha[\partial\mathbf{E}/\partial x] = \alpha[\mathbf{E}] - \alpha[x] = -2$ equals to $\alpha[f_\mathrm{i}] = \alpha[f_\mathrm{e}] = -2$, which indicates that the Poisson equation also follows the similarity scaling. Similarly, for the electron current density its scaling factor is $\alpha[\mathbf{J}_\mathrm{e}] = \alpha[n_\mathrm{e}] + \alpha[\mathbf{v}_\mathrm{e}] = -2$, where $\alpha[n_\mathrm{e}] = -2$ and $\alpha[\mathbf{v}_\mathrm{e}] = 0$; so is the case for the ion and total current density, i.e., $\alpha[\mathbf{J}_\mathrm{i}] = \alpha[\mathbf{J}_\mathrm{tot}] = -2$. Further, for rf discharge plasmas, since $\alpha[f] = \alpha[1/t] = -1$, the external driving frequency f should be tuned to keep the solution invariance, which indicates that the reduced frequency f/p should be constant or as a similarity invariant in compared systems, i.e., $\alpha[f/p] = 0$. Here, mathematically, the similarity theory is self-consistently interpreted from the Boltzmann and Poisson equations with universality, which can be applied to rf discharge plasmas.

A schematic of two similar discharge systems (S, S$^\#$) having different dimensional scales is shown in Fig. 1(a), and $G(x,t)$ is the physical parameter at the corresponding spatiotemperal point. We hereby make a statement to distinguish the similarity and scaling laws. The former hold with multiple control parameters scaled simultaneously, e.g., maintaining the similarity invariants pd and f/p to achieve similar rf discharges. The later usually determine the discharge parameter dependence on only one of the controlled parameters, e.g., discharge characteristics scaling with gas pressure [36, 37], gap dimension [38, 39], and driving frequency [40], respectively. As illustrated in Fig. 1(b), the scaling laws establish the parameter dependence of plasmas from S_1 to S_n [or from ($S_1^\#$ to $S_n^\#$)] whereas the similarity laws correlate the plasmas between (S_1, S_n) and $(S_1^\#, S_n^\#)$. Strategically, with the similarity laws being valid, discharge properties in S can be directly applied to $S^\#$ and vice versa, thus the conventional scaling laws can be exactly extrapolated from one system to another, enabling extended prediction parameter regimes in various rf plasma systems.

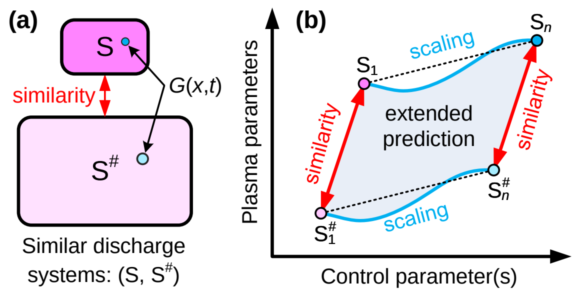

Figure 1. (a) Schematic of the similar discharge systems (S, $S^\#$) at different dimension scales. (b) A strategy showing the plasma property can be predicted in extended range of parameter regimes combining both the scaling and similarity laws.

In the following, PIC simulations are employed to demonstrate the applicability of the similarity laws for rf discharge plasma across the AG, SO, and BRH nonlinear transition regimes. The simulations of rf plasmas are performed with argon at 300 K, accounting for three electron-neutral collisions (elastic, excitation, and ionization scattering) and two ion-neutral collisions (isotropic and backward scattering) [41]. The custom developed electrostatic PIC code, ASTRA, is used for all the simulations (see [42] for the code benchmark with Turner *et al.* [43] and other details). Argon ions and electrons are tracked as particles. The rf plasmas are geometrically symmetric between two parallel-plate electrodes for simplicity. The rf voltage waveform $V_{\rm rf}(t) = V_{\rm rf} \cdot \sin(2\pi f t)$ [unit in Volt], where $f = 1/T$ is the driving frequency with T being the rf period, is connected to the powered electrode ($x = 0$) while the other electrode ($x = d$) is grounded. To satisfy the similar discharge conditions, the gas pressure p, gap distance d, and driving frequency f are simultaneously tuned with the scaling factor k, i.e., $k = p_k/p_1 = d_1/d_k = f_k/f_1$, keeping f/p and pd constant in compared systems. The emission coefficient of the ion induced secondary electron is $\gamma_{\rm se} = 0.1$ when it is considered and the electron reflection probability is $\gamma_{\rm re} = 0.2$ for all cases [44]. In the simulations, an implicit algorithm and an energy conservation scheme are adopted; the grid number and time step are case dependent while most of the cases are with 300 grid points and 2000 time steps per rf period.

III. RESULTS AND DISCUSSION

We demonstrate the similarity in rf discharges during the AG mode transition in Fig. 2. In the simulations, we set $[p, d, f] = [0.3\ \text{Torr}, 6.7\ \text{cm}, 13.56\ \text{MHz}]$ in S and $[p, d, f] = [0.6\ \text{Torr}, 3.35\ \text{cm}, 27.12\ \text{MHz}]$ in $S^\#$ with the scaling factor $k = 2$ and have $\gamma_{\rm se} = 0.1$ for all cases. The AG mode transitions are obtained by varying $V_{\rm rf}$ from 100 V to 1000 V, i.e., ten cases AG1–AG10 in S and $S^\#$, respectively [see Fig. 2(a)]. The transition occurs around the critical voltage $V_{\rm rf} = 500$ V, before and after which the time-averaged bulk electron density $n_{\rm e}$ versus $V_{\rm rf}$ shows two distinctly different scaling laws. The slope in the gamma mode is much higher than that in the alpha mode, which is also consistent with the experimental results by Godyak *et al.* [24] and simulation results by Boeuf *et al.* [45]. Most importantly, the electron density scaling S^+, which is extrapolated from S using $n_{\rm e}/k^2$, superimposes over that in $S^\#$. This indicates that the AG mode transition, though nonlinear, can be exactly replicated from one system to another. The spatiotemporal distributions of electron neutral elastic collision rates, $R_{\rm el} = K_{\rm el} n_{\rm e} N_{\rm n}$, where $K_{\rm el}$ the reaction rate coefficient, normalized to their maximums in S and $S^\#$ with $V_{\rm rf} = 500$ V (case AG5), respectively, are found to be the same [see Figs. 2(b) and 2(c)]. It is confirmed that the similarities hold in a dynamical manner with the time domain scaled correspondingly. The corresponding time-averaged scaled reaction rates normalized to the gas number density, i.e., $R_{\rm el}^{\rm n} = k^{-2} R_{\rm el} N_{\rm n}^{-1}$, are also exactly the same in S and $S^\#$ [see Fig. 2(d)], which explicitly confirms $\alpha[R_{\rm el}^{\rm n}] = \alpha[n_{\rm e}] = -2$ and quantitatively validates similarity laws in the compared rf plasma systems.

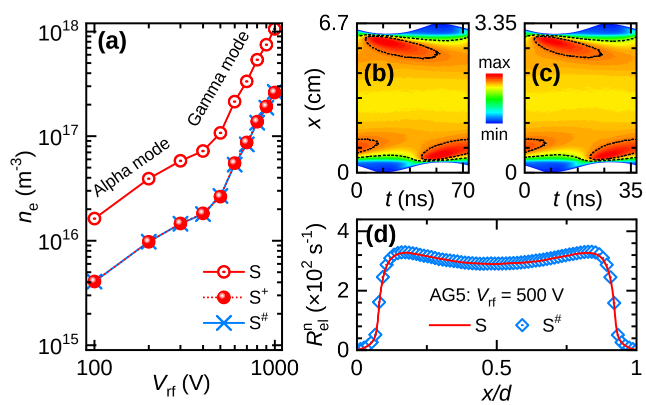

Figure 2. (a) Bulk electron density versus $V_{\rm rf}$ under similar discharge conditions during the AG mode transition. In the simulations, we set $[p, d, f] = [0.3\ \text{Torr}, 6.7\ \text{cm}, 13.56\ \text{MHz}]$ for S and $[p, d, f] = [0.6\ \text{Torr}, 3.35\ \text{cm}, 27.12\ \text{MHz}]$ for $S^\#$ with $\gamma_{\rm se} = 0.1$. Taking $V_{\rm rf} = 500$ V (case AG5) as an example to demonstrate the dynamical similarities: (b)–(c) Spatiotemporal distributions of the elastic collision rates normalized to their maximums in S and $S^\#$, respectively; (d) time-averaged scaled rates across the gap.

Electron power absorption (or electron heating), as a widely studied phenomenon, is essential for the deep understanding of fundamental behaviors of the rf discharge plasmas. Since the electron power absorption is expressed as $P_{\mathrm{e}} = \mathbf{J}_{\mathrm{e}} \cdot \mathbf{E}$, and according to the previous discussion, we have $\alpha[P_{\mathrm{e}}] = \alpha[\mathbf{J}_{\mathrm{e}}] + \alpha[\mathbf{E}] = -3$, which indicates that $k^{-3}P_{\mathrm{e}}$ should be invariant in similar rf discharges. It is generally considered that low-pressure rf plasmas are maintained by stochastic heating while at higher pressures the dominant heating is Ohmic, thus the SO mode transition can be observed by tuning the gas pressure [19]. Note that the stochastic heating is previously called collisionless heating, which may not be accurate. According to the studies [46–48] in more recent years, it has been recognized that collisions are needed to break the phase coherence between the electron motion and rf electric fields, resulting in net heating during one rf cycle, and at low-pressures this occurs by nonlocal collisions whereby collisions occur at a different spatial location to energy gain by the rf fields. Therefore, more exactly, the conventional collisionless heating should be understood as nonlocal collisional heating, also known as pressure heating. From the PIC simulations, the SO mode transition of the heating mechanisms is observed at different pressures; meanwhile, the applicability of the similarity laws for the rf plasma is examined.

We ran seven pressure-dependent cases (SO1–SO7) in the range of p/k = 0.01–1 Torr, with $k = 1$ in S and $k = 2$ in S$^{\#}$. It is observed that the electron density n_{e} increases as the gas pressure p increases with V_{rf} = 300 V and $\gamma_{\mathrm{se}} = 0.1$ used for all cases. Figure 3 shows the discharge similarity when the dominant electron power absorption transits from stochastic to Ohmic heating. The overlapping of the scaled electron density curves, S^{+} and S$^{\#}$, confirms the validity of the similarity factor $\alpha[n_{\mathrm{e}}] = -2$ [see Fig. 3(a)] during the SO transition. To further examine the electron heating mode, we decompose the electron power absorption P_{e} into the stochastic heating $P_{\mathrm{e,st}}$ and Ohmic heating $P_{\mathrm{e,Ohm}}$, i.e., $P_{\mathrm{e}} = P_{\mathrm{e,st}} + P_{\mathrm{e,Ohm}}$, based on the moment analysis of the electron Boltzmann equation [46, 48–50]. The $P_{\mathrm{e,Ohm}}/P_{\mathrm{e,st}}$ ratios in S and S$^{\#}$ are shown in Figure 3(b), which unambiguously demonstrates that the transitions from stochastic to Ohmic heating with increasing gas pressure overlap in similar discharge systems $(\mathrm{S}, \mathrm{S}^{\#})$. We take two cases of $p/k = 0.01$ Torr (SO1) and $p/k = 1$ Torr (SO7) as examples to further confirm the similarity in the spatial distribution of electron power absorption. In Fig. 3(c), the scaled electron power absorption, $k^{-3}P_{\mathrm{e}}$, at 0.01 Torr in S and 0.02 Torr in S$^{\#}$ are the same with the dominant electron heating rate being stochastic within the averaged sheath and the bulk Ohmic heating being neglectable. Figure 3(d) shows the same scaled total electron power absorption in SO7, i.e., 1 Torr in S and 2 Torr in S$^{\#}$, with the Ohmic heating being dominant. In comparison with Fig. 3(c), the magnitude of electron heating rates are largely increased, and there are significant positive electron heating in the bulk region. Figure 3(e) demonstrates the decomposed electron heating rates corresponding to Fig. 3(d), with correspondingly the same scaled stochastic and Ohmic heating components in S and S$^{\#}$, respectively. Also note $P_{\mathrm{e,Ohm}} > P_{\mathrm{e,st}}$ holds across the gap. Thus the similarity laws apply in rf plasmas dominated by either stochastic or Ohmic heating as well as the transition regimes.

Under certain conditions, electrons can be bounced back and forth many times between rf sheath fields and contiguously accelerated without experiencing collision, operating in the BRH mode, which is considered as a typical nonlinear mechanism in rf plasmas [27–29]. Here we examine the BRH nonlinear transition with $V_{\mathrm{rf}} = 40$ V and $\gamma_{\mathrm{se}} = 0$ under similar discharge conditions. The discharge condition parameters are $[p, f] = [0.025\ \mathrm{Torr}, 13.56\ \mathrm{MHz}]$ in S and $[p, f] = [0.05\ \mathrm{Torr}, 27.12\ \mathrm{MHz}]$ in S$^{\#}$. The BRH mode transitions are identified by tuning the gap distance, i.e., d = (2.5 cm, 1.25 cm), (4.5 cm, 2.25 cm), and (5 cm, 2.5 cm) for (S, S$^{\#}$), respectively. The temporal evolutions of the electron kinetic energy $\varepsilon_{\mathrm{e}}(t)$ from test particle simulations are shown in Figs. 4(a)–4(c), which demonstrate the gradual transition across the BRH mode. The test particle simulations are conducted using the spatiotemporal electric fields from PIC simulations of the rf discharges at steady state. Under the BRH condition [see Fig. 4(b)] the electron energy is highly enhanced up to 9 eV whereas $\varepsilon_{\mathrm{e}}(t)$ is generally less than 3 eV when BRH is less significant [see Figs. 4(a) and 4(c)]. Note that the efficiency of the demonstrated BRH mode is even higher than that by Park *et al.* [27] since the discharge condition parameters in BRH are further optimized. Although the BRH mode and its transition are considered to be nonlinear, this phenomenon can actually be reproduced in similar discharge systems. The corresponding normalized trajectories of the test particles, $k \cdot x(t)/d$, where $x(t)$ is the temporal position of the test particle, are also overlapping in S and S$^{\#}$ [see Figs. 4(d)–4(f)], which ensures the applicability of similarity laws in rf plasmas during the BRH mode transitions.

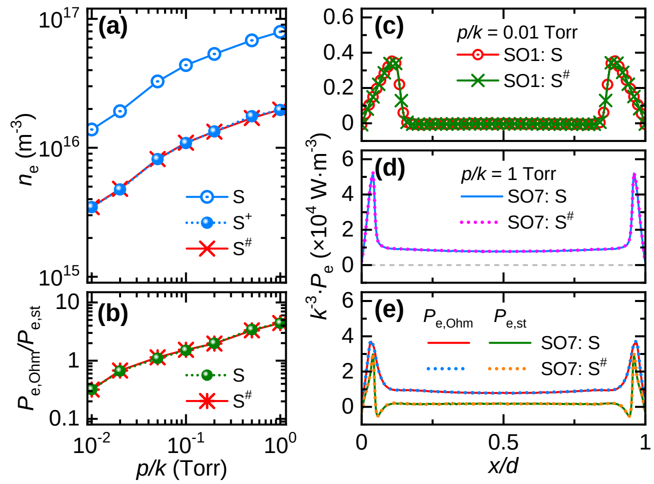

Figure 3. Discharge similarity in rf plasmas with an electron heating transition from stochastic to Ohmic regimes. (a) Bulk electron density and (b) the corresponding ratios between the Ohmic and stochastic heating components in similar discharge systems with p/k from 0.01 to 1 Torr. Time-averaged spatial distributions of the electron heating rate at (c) $p/k = 0.01$ Torr (SO1, stochastic heating dominated) and (d) $p/k = 1$ Torr (SO7, Ohmic heating dominated). (e) Decomposition of the electron heating rate in S and S$^{\#}$ at $p/k = 1$ (SO7). In the simulations, we have $V_{\mathrm{rf}} = 300$ V and $\gamma_{\mathrm{se}} = 0.1$ for all cases, and set $[d, f] = [6.7\ \mathrm{cm}, 13.56\ \mathrm{MHz}]$ in S and $[d, f] = [3.35\ \mathrm{cm}, 27.12\ \mathrm{MHz}]$ in S$^{\#}$, respectively.

We further examine the electron kinetic behaviors in rf plas-

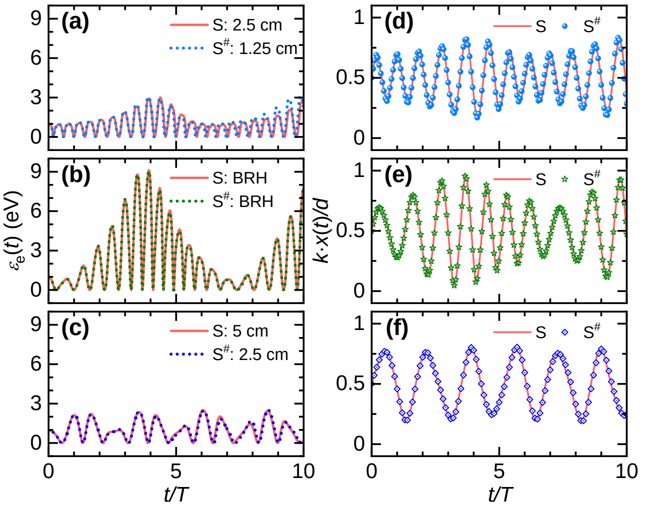

Figure 4. Determining the BRH mode transition by tuning the gap distance using test particle simulations. The gap distances are (a) (2.5 cm, 1.25 cm), (b) (4.5 cm, 2.25 cm) (under the BRH condition), and (c) (5 cm, 2.5 cm) in (S, S$^\#$), respectively. (d)–(f) Spatiotemporal electron trajectories corresponding to (a)–(c). In the simulations, we have $[p, f] = [0.025\ \text{Torr}, 13.56\ \text{MHz}]$ in S and $[p, f] = [0.05\ \text{Torr}, 27.12\ \text{MHz}]$ in S$^\#$, respectively, with $V_{\text{rf}} = 40$ V and the secondary electrons neglected ($\gamma_{\text{se}} = 0$) for all cases.

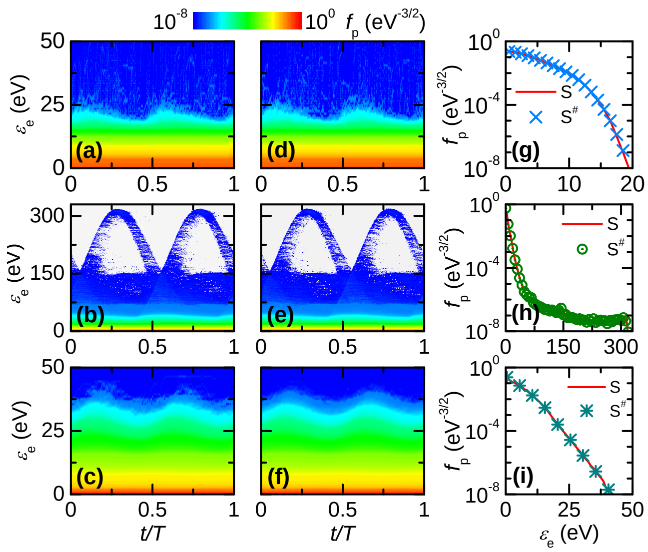

Figure 5. Electron kinetic invariance under similar discharge conditions. Temporal EEPFs in full space corresponding to (a) AG1, (b) SO1, (c) BRH in S and (d) AG1, (e) SO1, (f) BRH in S$^\#$. (g)–(i) Time-averaged EEPFs in S and S$^\#$ under similar discharge conditions.

mas under similar discharge conditions. As mentioned before, we have $\alpha[f_e/n_e] = \alpha[f_e] - \alpha[n_e] = 0$ in similar discharges, thus the normalized electron distribution function f_e/n_e should be an invariant. Converting f_e to the normalized electron energy probability function (EEPF) f_p using $\sqrt{\varepsilon} f_p(\varepsilon)\mathrm{d}\varepsilon = 4\pi \mathbf{v}^2 f_e(\mathbf{v})\mathrm{d}\mathbf{v}/n_e$, from Eq.(1) we have $\alpha[f_p] = \alpha[f_e/n_e] = 0$, which concludes that the EEPF is also invariant. The temporal and time-averaged EEPFs in full space under various similar discharge conditions are shown in Figure 5. In Figs. 5(a)–5(c), we show the temporal EEPFs in (a) the alpha mode with $V_{\text{rf}} = 100$ V (AG1), (b) stochastic heating dominated mode at p/k of 0.01 Torr (SO1), and (c) BRH mode at gap length of 4.5 cm in S. Figure 5(d)–5(f) show the corresponding EEPFs in S$^\#$ under similar discharge conditions. Although the EEPFs in different discharge modes are quite different, the distributions are the same in similar discharge systems. Figure 5(g)–5(i) show the time-averaged EEPFs in S and S$^\#$, which further confirms the invariance of the electron kinetics in similar discharges. It is also noteworthy that in Figs. 5(b) and 5(e) the wavy trajectories are due to secondary electrons, which have been characterized as high energy ballistic electrons [51]. These electrons are accelerated across the sheath ballistically and obtain the full potential energy, converting to the kinetic energy, and the maximum energy is close to the gap voltage ($V_{\text{rf}} = 300$ V) plus the plasma potential. Here the electron kinetics invariance, holding for electrons from different energy groups, is of the fundamental importance, which guarantees the similarity laws under various discharge conditions.

Our results confirmed that the nonlinear transition behaviors in rf plasmas can be exactly replicated under similar discharge conditions by simultaneously tuning the external discharge parameters $[p, d, f]$, keeping pd and f/p constant in the compared systems. Physically, $pd \propto d/\lambda \sim N_{\text{coll}}$ (λ is the mean free path), represents the electron mean collision times across the gap, and $f/p \propto f/\nu_{\text{coll}} = T^{-1}/\tau_{\text{coll}}^{-1} \sim N_{\text{coll}}^{-1}$ ($\nu_{\text{coll}} = \tau_{\text{coll}}^{-1} \propto p$ is the electron collision frequency), indicates an inverse of the electron mean collision times during one rf cycle. Since pd and f/p are kept constant under similar discharge conditions, $fd = pd \times f/p$ is also maintained, which is a well-known similarity parameter for multipactor discharges that usually occur in vacuum or at rather low pressure where the pressure effect is not typically considered [17, 52]. The three combined parameters are not independent and any two of them can be chosen and can work equivalently; here pd and f/p are selected since the pressure effect is critical for rf discharge plasmas. Although the kinetic interpretations are no longer based on local-field approximations, the reduced electric field E/p is still a similarity invariant here, which holds for the separated electric field components, e.g., electrostatic field and the space charge field, as well as the total electric field, in similar rf discharges. The ideas of similarity scalings are somewhat similar to the Buckingham π-theorem [53], both of which can be used to reduce the number of independent parameters for describing physically similar systems [5]. We would like to further emphasize that the similarity laws are more useful in extrapolating discharge parameters among the similar discharge systems, whereas the π-theorem is also typically utilized for dimensional analysis.

In the present work the similarity laws are demonstrated with the scaling factor $k = 2$ and one-dimensional geometry. The similarity properties are also expected with a larger scaling factor or for higher dimensional geometrically similar systems when the fundamental physical processes are maintained. For example, similar rf discharges can still be obtained in compared systems with $k = 10$ [31]. However, with a larger k the scaled rf discharge parameters may enter into high-pressure and high ionization degree regimes, in which other collision processes (e.g., stepwise ionizations and Coulomb collisions [54]) could be important and their effects need further investigations. Also, currently the results are for atomic gases only while for the electronegative or molecular gases, the scaling laws could be more complicated since the negative ions and ion-ion recombination should be additionally considered.

IV. CONCLUSION

We have generalized and demonstrated the similarity laws for rf plasmas across various nonlinear transition regimes, based on theoretical interpretations and fully kinetic particle simulations. From the perspective of the similarity theory, the nonlinear transition behaviors, such as the AG, SO, and BRH mode transitions, can be exactly replicated in similar discharge systems, and thus the scaling laws during the transition can be extrapolated from one system to another. The fundamental mechanisms, such as the electron kinetic invariance, for maintaining the similarity laws are elucidated based on the scaling and solution invariance of the Boltzmann equations and the coupled Poisson equation. The results from this work bring comprehensive insights and additional flexibility for plasma characterizations towards extended parameter regimes, which provide valuable guidance in developing up-scaling plasma devices, e.g., next generation plasma processing facilities for etching applications. Moreover, the generalization of similarity laws also suggests a strategy with scale reduction for large-scale simulations when the model equations could be treated as absolute invariants. The effects of the stepwise ionizations at high pressures, the Coulomb collisions toward highly ionized regimes, and possible electromagnetic mechanisms [55, 56] at high frequencies, as well as the applicability of the similarity laws in electronegative gas discharge plasmas [57–59], will be explored in the future work.

ACKNOWLEDGMENTS

This work is supported by the State Key Laboratory of Power System and Generation Equipment at Tsinghua University Project No. SKLD21M06. B.Z. and Q.H.F. acknowledge funding support from the National Science Foundation Grant Nos. 1917577 and 1724941 in the United States. J.P.V. acknowledges funding support from the U.S. Department of Energy Office of Fusion Energy Science Grant No. DE-SC0001939. P.Z. acknowledges funding support from the Air Force Office of Scientific Research YIP Grant No. FA9550-18-1-0061. J.P.V. and P.Z. also acknowledge funding support from the Air Force Office of Scientific Research Grant No. FA9550-18-1-0062 and the U.S. Department of Energy Office of Science Grant No. DE-SC0022078. Y.F. and H.W. contributed equally to this work.

[1] D. Janasek, J. Franzke, and A. Manz, Scaling and the design of miniaturized chemical-analysis systems, Nature **442**, 374 (2006).
[2] D. D. Ryutov, Scaling laws for dynamical plasma phenomena, Phys. Plasmas **25**, 100501 (2018).
[3] Y. Fu and J. P. Verboncoeur, On the similarities of low-temperature plasma discharges, IEEE Trans. Plasma Sci. **47**, 1994 (2019).
[4] J. P. Sauppe, S. Palaniyappan, B. J. Tobias, J. L. Kline, K. A. Flippo, O. L. Landen, D. Shvarts, S. H. Batha, P. A. Bradley, E. N. Loomis, N. N. Vazirani, C. F. Kawaguchi, L. Kot, D. W. Schmidt, T. H. Day, A. B. Zylstra, and E. Malka, Demonstration of Scale-Invariant Rayleigh-Taylor Instability Growth in Laser-Driven Cylindrical Implosion Experiments, Phys. Rev. Lett. **124**, 185003 (2020).
[5] D. Michael, M. Khodorkovskii, A. Pastor, N. Timofeev, and G. Zissis, Application of similarity laws as a light source diagnostics, J. Phys. D: Appl. Phys. **43**, 234005 (2010).
[6] A. von Engel, *Ionized Gases* (Clarendon, Oxford, 1965).
[7] T. M. P. Briels, E. M. Van Veldhuizen, and U. Ebert, Positive streamers in air and nitrogen of varying density: experiments on similarity laws, J. Phys. D: Appl. Phys. **41**, 234008 (2008).
[8] G. A. Mesyats, Similarity laws for pulsed gas discharges, Phys.-Usp. **49**, 1045 (2006).
[9] P. Osmokrović, T. Živić, B. Lončar, and A. Vasić, The validity of the general similarity law for electrical breakdown of gases, Plasma Sources Sci. Technol. **15**, 703 (2006).
[10] C. C. Petty, Sizing up plasmas using dimensionless parameters, Phys. Plasmas **15**, 080501 (2008).
[11] N. Liu and V. P. Pasko, Effects of photoionization on similarity properties of streamers at various pressures in air, J. Phys. D: Appl. Phys. **39**, 327 (2006).
[12] V. P. Pasko, Red sprite discharges in the atmosphere at high altitude: the molecular physics and the similarity with laboratory discharges, Plasma Sources Sci. Technol. **16**, S13 (2007).
[13] F. Paschen, Ueber die zum Funkenübergang in Luft, Wasserstoff und Kohlensäure bei verschiedenen Drucken erforderliche Potentialdifferenz, Ann. Phys. **273**, 69 (1889).
[14] J. S. Townsend, *Electricity in Gases* (Clarendon, Oxford, 1915).
[15] H. Margenau, Theory of high frequency gas discharges. IV. Note on the similarity principle, Phys. Rev. **73**, 326 (1948).
[16] F. L. Jones and G. D. Morgan, High-frequency discharges: I Breakdown mechanism and similarity relationship, Proc. Phys. Soc. Lond. B **64**, 560 (1951).
[17] V. Lisovskiy, J. P. Booth, K. Landry, D. Douai, V. Cassagne, and V. Yegorenkov, Similarity law for rf breakdown, Europhys. Lett. **82** (2008).
[18] M. A. Lieberman and A. J. Lichtenberg, *Principles of Plasma Discharges and Materials Processing* (New York: John Wiley & Sons, 2005).
[19] P. Chabert and N. Braithwaite, *Physics of Radio-Frequency Plasmas* (Cambridge: Cambridge University Press, 2011).
[20] M. Puač, D. Marić, M. Radmilović-Radjenović, M. Šuvakov, and Z. L. Petrović, Monte carlo modeling of radio-frequency

breakdown in argon, Plasma Sources Sci. Technol. **27**, 075013 (2018).

[21] M. U. Lee, J. Lee, J. K. Lee, and G. S. Yun, Extended scaling and Paschen law for micro-sized radiofrequency plasma breakdown, Plasma Sources Sci. Technol. **26**, 034003 (2017).

[22] A. M. Loveless and A. L. Garner, Scaling laws for AC gas breakdown and implications for universality, Phys. Plasmas **24**, 1 (2017).

[23] Y. Fu, B. Zheng, D.-Q. Wen, P. Zhang, Q. H. Fan, and J. P. Verboncoeur, Similarity law and frequency scaling in low-pressure capacitive radio frequency plasmas, Appl. Phys. Lett. **117**, 204101 (2020).

[24] V. A. Godyak, R. B. Piejak, and B. M. Alexandrovich, Measurement of electron energy distribution in low-pressure rf discharges, Plasma Sources Sci. Technol. **1**, 36 (1992).

[25] I. D. Kaganovich, V. I. Kolobov, and L. D. Tsendin, Stochastic electron heating in bounded radio-frequency plasmas, Appl. Phys. Lett. **69**, 3818 (1996).

[26] M. M. Turner and P. Chabert, Collisionless heating in capacitive discharges enhanced by dual-frequency excitation, Phys. Rev. Lett. **96**, 205001 (2006).

[27] G. Y. Park, S. J. You, F. Iza, and J. K. Lee, Abnormal heating of low-energy electrons in low-pressure capacitively coupled discharges, Phys. Rev. Lett. **98**, 085003 (2007).

[28] Y.-X. Liu, Q.-Z. Zhang, W. Jiang, L.-J. Hou, X.-Z. Jiang, W.-Q. Lu, and Y.-N. Wang, Collisionless bounce resonance heating in dual-frequency capacitively coupled plasmas, Phys. Rev. Lett. **107**, 055002 (2011).

[29] T. Mussenbrock, R. P. Brinkmann, M. A. Lieberman, A. J. Lichtenberg, and E. Kawamura, Enhancement of ohmic and stochastic heating by resonance effects in capacitive radio frequency discharges: A theoretical approach, Phys. Rev. Lett. **101**, 085004 (2008).

[30] A. A. Rukhadze, N. N. Sobolev, and V. V. Sokovikov, Similarity relations for low-temperature nonisothermal discharges, Sov. Phys. Usp. **34**, 827 (1991).

[31] Y. Fu, B. Zheng, P. Zhang, Q. H. Fan, J. P. Verboncoeur, and X. Wang, Similarity of capacitive radio-frequency discharges in nonlocal regimes, Phys. Plasmas **27**, 113501 (2020).

[32] F. Iza, J. K. Lee, and M. G. Kong, Electron kinetics in radio-frequency atmospheric-pressure microplasmas, Phys. Rev. Lett. **99**, 075004 (2007).

[33] G. J. M. Hagelaar and L. C. Pitchford, Solving the Boltzmann equation to obtain electron transport coefficients and rate coefficients for fluid models, Plasma Sources Sci. Technol. **14**, 722 (2005).

[34] C. E. Muehe, Scaling laws for high-density plasmas, J. Appl. Phys. **45**, 82 (1974).

[35] J. A. Bittencourt, *Fundamentals of Plasma Physics* (Springer Science & Business Media, New York, 2004).

[36] M. Vass, S. Wilczek, T. Lafleur, R. P. Brinkmann, Z. Donkó, and J. Schulze, Observation of dominant ohmic electron power absorption in capacitively coupled radio frequency argon discharges at low pressure, Plasma Sources Sci. Technol. **29**, 085014 (2020).

[37] Y. Fu, P. Zhang, J. P. Verboncoeur, and X. Wang, Electrical breakdown from macro to micro/nano scales: a tutorial and a review of the state of the art, Plasma Res. Express **2**, 013001 (2020).

[38] K. Bera, S. Rauf, K. Ramaswamy, and K. Collins, Effects of interelectrode gap on high frequency and very high frequency capacitively coupled plasmas, J. Vac. Sci. Technol. A **27**, 706 (2009).

[39] A. M. Loveless and A. L. Garner, Scaling laws for gas breakdown for nanoscale to microscale gaps at atmospheric pressure, Appl. Phys. Lett. **108**, 234103 (2016).

[40] S. Sharma, N. Sirse, M. M. Turner, and A. R. Ellingboe, Influence of excitation frequency on the metastable atoms and electron energy distribution function in a capacitively coupled argon discharge, Phys. Plasmas **25**, 063501 (2018).

[41] B. Zheng, Y. Fu, D. Q. Wen, K. Wang, T. Schuelke, and Q. H. Fan, Influence of metastable atoms in low pressure magnetized radio-frequency argon discharges, J. Phys. D: Appl. Phys. **53** (2020).

[42] B. Zheng, K. Wang, T. Grotjohn, T. Schuelke, and Q. H. Fan, Enhancement of ohmic heating by hall current in magnetized capacitively coupled discharges, Plasma Sources Sci. Technol. **28**, 09LT03 (2019).

[43] M. M. Turner, A. Derzsi, Z. Donkó, D. Eremin, S. J. Kelly, T. Lafleur, and T. Mussenbrock, Simulation benchmarks for low-pressure plasmas: Capacitive discharges, Phys. Plasmas **20**, 013507 (2013).

[44] M. Daksha, A. Derzsi, S. Wilczek, J. Trieschmann, T. Mussenbrock, P. Awakowicz, Z. Donkó, and J. Schulze, The effect of realistic heavy particle induced secondary electron emission coefficients on the electron power absorption dynamics in single- and dual-frequency capacitively coupled plasmas, Plasma Sources Sci. Technol. **26**, 085006 (2017).

[45] P. Belenguer and J. P. Boeuf, Transition between different regimes of rf glow discharges, Phys. Rev. A **41**, 4447 (1990).

[46] T. Lafleur, P. Chabert, and J. P. Booth, Electron heating in capacitively coupled plasmas revisited, Plasma Sources Sci. Technol. **23**, 035010 (2014).

[47] T. Lafleur and P. Chabert, Is collisionless heating in capacitively coupled plasmas really collisionless?, Plasma Sources Sci. Technol. **24**, 044002 (2015).

[48] J. Schulze, Z. Donkó, T. Lafleur, S. Wilczek, and R. P. Brinkmann, Spatio-temporal analysis of the electron power absorption in electropositive capacitive RF plasmas based on moments of the Boltzmann equation, Plasma Sources Sci. Technol. **27**, 055010 (2018).

[49] M. Surendra and M. Dalvie, Moment analysis of rf parallel-plate-discharge simulations using the particle-in-cell with monte carlo collisions technique, Phys. Rev. E **48**, 3914 (1993).

[50] R. P. Brinkmann, Electron heating in capacitively coupled RF plasmas: a unified scenario, Plasma Sources Sci. Technol. **25**, 014001 (2015).

[51] Y. Fu, B. Zheng, D.-Q. Wen, P. Zhang, Q. H. Fan, and J. P. Verboncoeur, High-energy ballistic electrons in low-pressure radio-frequency plasmas, Plasma Sources Sci. Technol. **29**, 09LT01 (2020).

[52] R. Woo and A. Ishimaru, A similarity principle for multipacting discharges, J. Appl. Phys. **38**, 5240 (1967).

[53] E. Buckingham, On physically similar systems; illustrations of the use of dimensional equations, Phys. Rev. **4**, 345 (1914).

[54] G. J. Hagelaar, Z. Donko, and N. Dyatko, Modification of the Coulomb Logarithm due to Electron-Neutral Collisions, Phys. Rev. Lett. **123**, 25004 (2019).

[55] M. A. Lieberman, J. P. Booth, P. Chabert, J. M. Rax, and M. M. Turner, Standing wave and skin effects in large-area, high-frequency capacitive discharges, Plasma Sources Sci. Technol. **11**, 283 (2002).

[56] K. Zhao, D.-Q. Wen, Y.-X. Liu, M. A. Lieberman, D. J. Economou, and Y. N. Wang, Observation of Nonlinear Standing Waves Excited by Plasma-Series-Resonance-Enhanced Harmonics in Capacitive Discharges, Phys. Rev. Lett. **122**, 185002 (2019).

[57] A. Proto and J. T. Gudmundsson, Electron power absorption in radio frequency driven capacitively coupled chlorine discharge, Plasma Sources Sci. Technol. **30**, 065009 (2021).

[58] J. T. Gudmundsson and A. Proto, Electron heating mode transitions in a low pressure capacitively coupled oxygen discharge, Plasma Sources Sci. Technol. **28**, 045012 (2019).

[59] J. Schulze, A. Derzsi, K. Dittmann, T. Hemke, J. Meichsner, and Z. Donkó, Ionization by drift and ambipolar electric fields in electronegative capacitive radio frequency plasmas, Phys. Rev. Lett. **107**, 275001 (2011).